Hybrid Composites

International Edition: DOI: 10.1002/anie.201604880
German Edition: DOI: 10.1002/ange.201604880

Engineering of $CH_3NH_3PbI_3$ Perovskite Crystals by Alloying Large Organic Cations for Enhanced Thermal Stability and Transport Properties

*Wei Peng, Xiaohe Miao, Valerio Adinolfi, Erkki Alarousu, Omar El Tall, Abdul-Hamid Emwas, Chao Zhao, Grant Walters, Jiakai Liu, Olivier Ouellette, Jun Pan, Banavoth Murali, Edward H. Sargent, Omar F. Mohammed, and Osman M. Bakr**

Abstract: *The number of studies on organic–inorganic hybrid perovskites has soared in recent years. However, the majority of hybrid perovskites under investigation are based on a limited number of organic cations of suitable sizes, such as methylammonium and formamidinium. These small cations easily fit into the perovskite's three-dimensional (3D) lead halide framework to produce semiconductors with excellent charge transport properties. Until now, larger cations, such as ethylammonium, have been found to form 2D crystals with lead halide. Here we show for the first time that ethylammonium can in fact be incorporated coordinately with methylammonium in the lattice of a 3D perovskite thanks to a balance of opposite lattice distortion strains. This inclusion results in higher crystal symmetry, improved material stability, and markedly enhanced charge carrier lifetime. This crystal engineering strategy of balancing opposite lattice distortion effects vastly increases the number of potential choices of organic cations for 3D perovskites, opening up new degrees of freedom to tailor their optoelectronic and environmental properties.*

The past several years have seen the emergence of organic–inorganic hybrid perovskites ABX_3 (where A is an organic cation, B is a metal cation, and X is a halide anion) as a new class of high-performance photovoltaic semiconductors.[1] While there is some flexibility in the choices of A, B, and X components, there is one principal requirement governing the allowed sizes of the precursor ions, which can be expressed as: $R_A + R_X = t\sqrt{2}(R_B + R_X)$, where R represents the corresponding ionic radii of the ions and t is the tolerance factor. To obtain a stable three-dimensional (3D) crystal structure, which is required for efficient charge transport, t should be between 0.8 to 1.[2] When $t > 1$, perovskites of low-dimension crystal structures will form, showing suppressed charge transport along the lattice direction perpendicular to the large organic cation layer.[2a] Interestingly, the mixture of both large and small organic cations can lead to the formation of perovskites of the so-called quasi-2D structure.[3] Yet, they still lag behind 3D perovskites from the transport perspective. However, quasi-2D perovskites display much higher ambient stability due to the weaker polarity and larger mass of the large organic cations. Finding a strategy to incorporate large organic cations into 3D perovskite structures would vastly expand the library of 3D perovskites with engineered properties, including desirable transport and stability.

$CH_3NH_3PbI_3$ ($MAPbI_3$) is the most widely studied 3D perovskite,[1] but it suffers from various instability issues.[4] $MAPbI_3$ was found to degrade gradually at 85 °C (as required by IEC 61646 climatic chamber tests) even in an inert atmosphere.[5] In addition, the phase transition of $MAPbI_3$ from cubic to tetragonal phases at ca. 57 °C[6] may cause undesired lattice strain and distortion, potentially harmful for device operation.[7] These intrinsic instability issues can be overcome only through materials design. Therefore, we sought to develop a strategy to engineer the properties of $MAPbI_3$ with large organic cations. It is worth pointing out that the inability of large organic cations to form stable 3D crystals may arise from two situations. First, cations with ionic radii that do not exceed the dimensions of the inorganic cuboctahedral holes yet still induce large lattice strain to make the formation of a 3D crystal thermodynamically unfavorable. Second, cations larger than the geometric limits of the inorganic framework, by any case, will not fit into the 3D lattice.[3] However, the former case may be circumvented through the choice of components so as to reduce the free energy of the targeted 3D structures. It was previously found that ethylammonium (EA) could not form 3D crystals with lead iodide because the associated tolerance factor is slightly larger than 1.[2b,8] This made it an ideal candidate for our study.

We started our work by growing EA-incorporated $MAPbI_3$ single crystals.[9] With an appropriate amount of

[*] W. Peng, Dr. E. Alarousu, J. Liu, Dr. J. Pan, Dr. B. Murali, Prof. O. F. Mohammed, Prof. O. M. Bakr
Division of Physical Sciences and Engineering
King Abdullah University of Science and Technology (KAUST)
Thuwal 23955-6900 (Saudi Arabia)
E-mail: osman.bakr@kaust.edu.sa
Dr. X. Miao, Dr. A. H. Emwas, Dr. C. Zhao
Imaging and Characterization Core Lab
King Abdullah University of Science and Technology (KAUST)
Thuwal 23955-6900 (Saudi Arabia)
Dr. O. El Tall
Analytical Core Lab
King Abdullah University of Science and Technology (KAUST)
Thuwal 23955-6900 (Saudi Arabia)
V. Adinolfi, G. Walters, O. Ouellette, Prof. E. H. Sargent
Department of Electrical and Computer Engineering, University of Toronto
Toronto, Ontario M5S 3G4 (Canada)

Supporting information for this article can be found under: http://dx.doi.org/10.1002/anie.201604880.

EA^+ additive in the $MAPbI_3$ crystallization precursor (see the Supporting Information), we grew crystals exhibiting a cubic shape and a metallic black color, contrasting with the truncated octahedral shape of $MAPbI_3$ single crystals (see Figure 1 a inset). To determine the phase of this new single crystal, we first acquired the X-ray diffraction (XRD) spectrum of ground crystal powders. As shown in Figure 1 a, the diffraction pattern can be indexed as a typical cubic crystal with a lattice constant of approximately 6.31 Å. The diffraction pattern of the tetragonal $MAPbI_3$ crystals is also shown in Figure 1 a for comparison. To gain a better understanding of the structure, single-crystal XRD was also performed. We solved the structure with a cubic symmetry in the $Pm\bar{3}m$ space group. The crystal lattice comprises a Pb–I framework with a bond length of 3.16 Å, resembling that of $MAPbI_3$ crystals in the cubic phase.[6a] Details of the crystal data can be found in Table S1. The simulated powder XRD pattern agrees well with our powder XRD result (Figure 1 a). Unfortunately, due to the much lower diffraction intensity of the organic components as well as their intense rotating motion, we could not resolve their distributions.[6c]

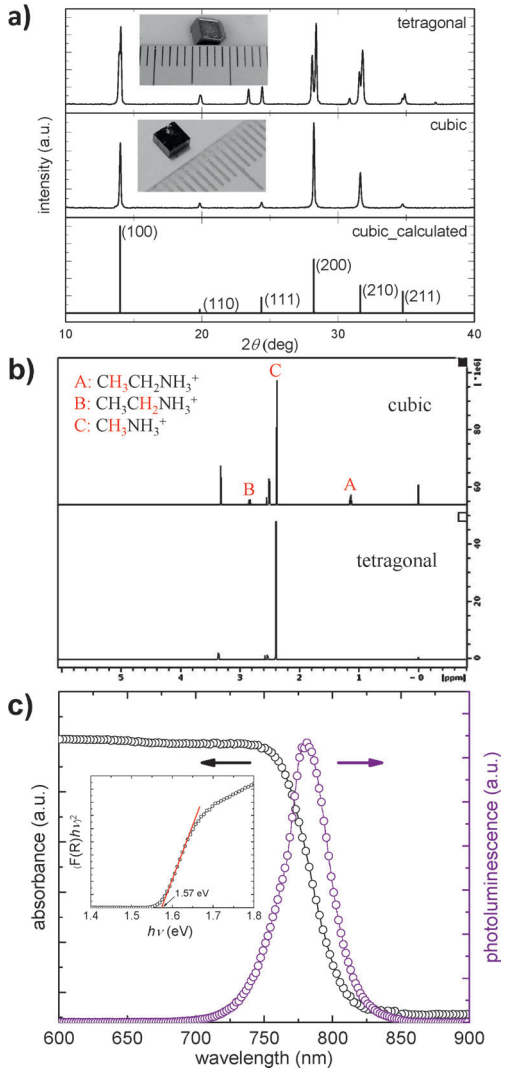

Figure 1. a) Powder XRD patterns of the tetragonal $MAPbI_3$ crystal and the cubic crystal, with photos of the single crystals in the inset. The XRD pattern calculated from the cubic crystal structure data is also presented. b) ^1H NMR spectra of the cubic and tetragonal samples. The species corresponding to the ^1H peaks are listed. c) The absorbance and the PL spectra of the cubic crystal. The inset shows the Tauc plot of the cubic crystal, indicating a band gap of 1.57 eV.

To determine the MA^+/EA^+ ratio of the cubic crystal, we performed elemental analysis with a CHN analyzer. Average mass fractions of 1.72 % and 2.20 % for C and N, respectively, were measured for $MAPbI_3$ crystal powders. This result agrees (within error) with theoretical values. As for the cubic crystal, the values are 2.04 % and 2.19 % for C and N, respectively, from which we can estimate a ratio of 0.23 for EA^+/MA^+. To further confirm the composition, we used solution-phase ^{13}C and ^1H NMR spectroscopy. From the ^{13}C NMR spectra (Figure S2), we can identify three ^{13}C species in the cubic sample, one of which can be also identified in the tetragonal sample. This agrees well with the corresponding proportions of carbon species in EA^+ and MA^+. ^1H NMR spectroscopy was then used to determine the composition quantitatively (Figure 1 b). The species corresponding to the ^1H peaks are listed on the graph. The integration of these peaks yields a A/B/C ratio of 1.00:0.68:5.00. The A/B ratio agrees well with the proton population ratio $-CH_3/-CH_2-$ in EA^+, and the A/C ratio indicates an EA/MA ratio of 1:5, in good accordance with the CHN analysis result. In light of this now well-defined composition, we use the formula $EA_{0.17}MA_{0.83}PbI_3$ hereafter to refer to the cubic crystals.

In contrast to $MAPbI_3$ with a small unit cell of high symmetry, $EAPbI_3$ was previously reported to crystallize in a 2D structure with a large orthorhombic unit cell.[8] This is due to the large ionic radius of EA^+, roughly 274 pm, compared to 217 pm for MA^+, resulting in a tolerance factor of 1.030, which is slightly out of the empirical range (0.8–1.0) for a stable 3D perovskite structure.[2b] In the present case, however, a relatively large number of EA^+ ions fit into the 3D structure of $MAPbI_3$. Considering that the size of EA^+ is close to the upper limit of the accepted tolerance factor range, we propose that the two lattice-distortion factors, including the small radius of MA^+ that causes lattice contraction and the large radius of EA^+ that causes lattice dilation, coordinately lead to a decrease of the free energy of the crystal system, and therefore the formation of a stable 3D PbI_6 octahedral framework.

We extracted a band gap of 1.57 eV for $EA_{0.17}MA_{0.83}PbI_3$ from its diffuse reflectance spectrum (Figure 1 c). The photoluminescence (PL) spectrum of the crystal is also shown. Notably, negligible differences are observed in both absorption and PL spectra compared with those of $MAPbI_3$ (see Figure S3). The retention of optical properties agrees with previous studies.[6a] From the perspective of light-absorbing capability, $EA_{0.17}MA_{0.83}PbI_3$ still holds potential as a suitable photovoltaic material.

We explored the phase transition of $EA_{0.17}MA_{0.83}PbI_3$ through temperature-dependent XRD. The powder XRD patterns were acquired at various temperatures from 80 to −130 °C. As shown in Figure 2 a, it is clear that $EA_{0.17}MA_{0.83}PbI_3$ retains its cubic structure over temperatures

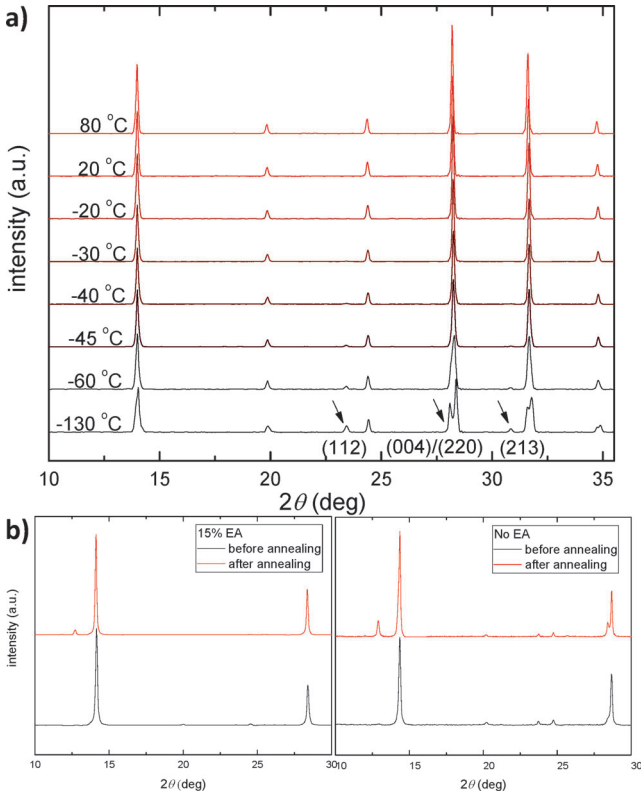

Figure 2. a) Temperature-dependent XRD patterns of $EA_{0.17}MA_{0.83}PbI_3$ crystal powders examined from −130 to 80 °C. b) XRD patterns of $MAPbI_3$ (without EA) and $EA_{0.17}MA_{0.83}PbI_3$ (with EA) thin films before and after 24 h annealing at 85 °C.

ranging from 80 to −30 °C. However, at temperatures below −30 °C, the diffraction features of a tetragonal crystal (indicated by the arrows in the plot) gradually emerge. This finding suggests a tetragonal–cubic phase transition at roughly −30 °C, which is much lower than that of $MAPbI_3$ (ca. 57 °C). This higher phase stability suggests a lower free energy and higher stability of the $EA_{0.17}MA_{0.83}PbI_3$ crystal.

The thermal stability of $EA_{0.17}MA_{0.83}PbI_3$ is expected to be higher than that of $MAPbI_3$, considering the different volatility of EA and MA.[10] To confirm our hypothesis, we prepared $MAPbI_3$ thin films with and without EA (see the Supporting Information). The as-prepared thin films were then annealed at 85 °C for 24 h in N_2. The films before and after annealing were checked with XRD (Figure 2b). Scanning electron microscopy (SEM) shows that both thin films comprise grains of similar sizes (Figure S4), ruling out grain sizes as a variable for stability comparison. After the annealing, both films show the diffraction of PbI_2, indicating decomposition of perovskites. The normalized diffraction patterns show stronger PbI_2 diffraction in the $MAPbI_3$ film that has a PbI_2/perovskite diffraction intensity ratio of (22.3 ± 8.2)% than the value of (9.8 ± 2.4)% in $EA_{0.17}MA_{0.83}PbI_3$. This finding clearly demonstrates the higher thermal stability of $EA_{0.17}MA_{0.83}PbI_3$ over $MAPbI_3$.

$MAPbI_3$ single crystals were previously reported with long carrier lifetimes, moderate carrier mobilities, and low trap densities, which are the most important optoelectronic properties.[9] We therefore used transient absorption (TA) spectroscopy to study the dynamic properties of the charge carriers in $EA_{0.17}MA_{0.83}PbI_3$.[11] The TA signal of the excited-state absorption of both the $EA_{0.17}MA_{0.83}PbI_3$ and the $MAPbI_3$ single crystals was captured at 850 nm in transmission mode to reduce the influence of surface defects (Figure 3a). A double-exponential decay can be fitted to both curves. The fast decay component has been ascribed to the crystal's surface contribution, while the slow decay component was considered as the contribution from the bulk.[9] Surprisingly, $EA_{0.17}MA_{0.83}PbI_3$ exhibits a bulk lifetime as long as 2000 ns, which constitutes a nearly 10-fold improvement compared to that in $MAPbI_3$ (300 ns).[12] We also carried out surface-sensitive PL decay measurements on the $EA_{0.17}MA_{0.83}PbI_3$ crystal (Figure S5), and revealed a relatively shorter carrier lifetime of ca. 300 ns, possibly due to the presence of abundant defects on the crystal surface originating from the drying of surface-detained precursor solution and/or ambient attacking factors.[9,12]

There are two plausible reasons for the increase of the carrier lifetime. First, a recent computational study showed the transition of perovskites' band structure from direct to indirect would happen with the MA rotation, thus suppressing carrier recombination.[13] It is then reasonable to speculate that the more rapid motion of MA^+ in a larger cubic unit cell (as in $EA_{0.17}MA_{0.83}PbI_3$) than in a distorted tetragonal unit cell (as in $MAPbI_3$) would enhance such a dynamic phenomenon and further charge separation. Second, spin–orbit coupling (SOC), a crucial factor influencing the electronic properties of hybrid perovskites, induces the Rashba effect.[14] This effect would also suppress carrier recombination.[14a] It was further found that SOC would be enhanced in a higher-symmetry crystal.[14b] From this aspect, $EA_{0.17}MA_{0.83}PbI_3$ may also display longer carrier lifetimes due to its improved crystal symmetry. In all, we propose that the fine tuning of the crystal structure may have led to the improved carrier dynamics.

We then used the space charge limited current (SCLC) method to study the defect states of $EA_{0.17}MA_{0.83}PbI_3$. The current–voltage (I–V) curve was measured from a hole-injecting device structure, Au/single crystal/Au, and an electron-injecting device, Au/Ti/single crystal/Ti/Au, as shown in Figure 3b,c. The voltage marking the transition from the Ohmic region ($n = 1$) to the trap-filled limit (TFL) region ($n > 3$), V_{TFL}, is used to calculate the trap densities close to the VBM and the CBM,[15] which are roughly 1.57×10^{10} cm^{-3} and 8.3×10^{10} cm^{-3}, respectively (see the Supporting Information). Average trap densities of $(3.3 \pm 0.5) \times 10^{10}$ cm^{-3} and $(8.0 \pm 0.5) \times 10^{10}$ cm^{-3} near the VBM and the CBM, respectively, were calculated based on five different crystals. The values are within the same order of magnitude of those found in $MAPbI_3$ (see Figure S6 and also previous reports),[9,16] demonstrating the high quality of this new material.

Furthermore, from the Child region ($n = 2$), we can extract the carrier mobility.[15] The average hole mobility and electron mobility were calculated to be (636 ± 201) $cm^2 V^{-1} s^{-1}$ and (17 ± 5) $cm^2 V^{-1} s^{-1}$, respectively. The electron mobility is similar as that of $MAPbI_3$, while the hole mobility is strikingly improved by almost one order

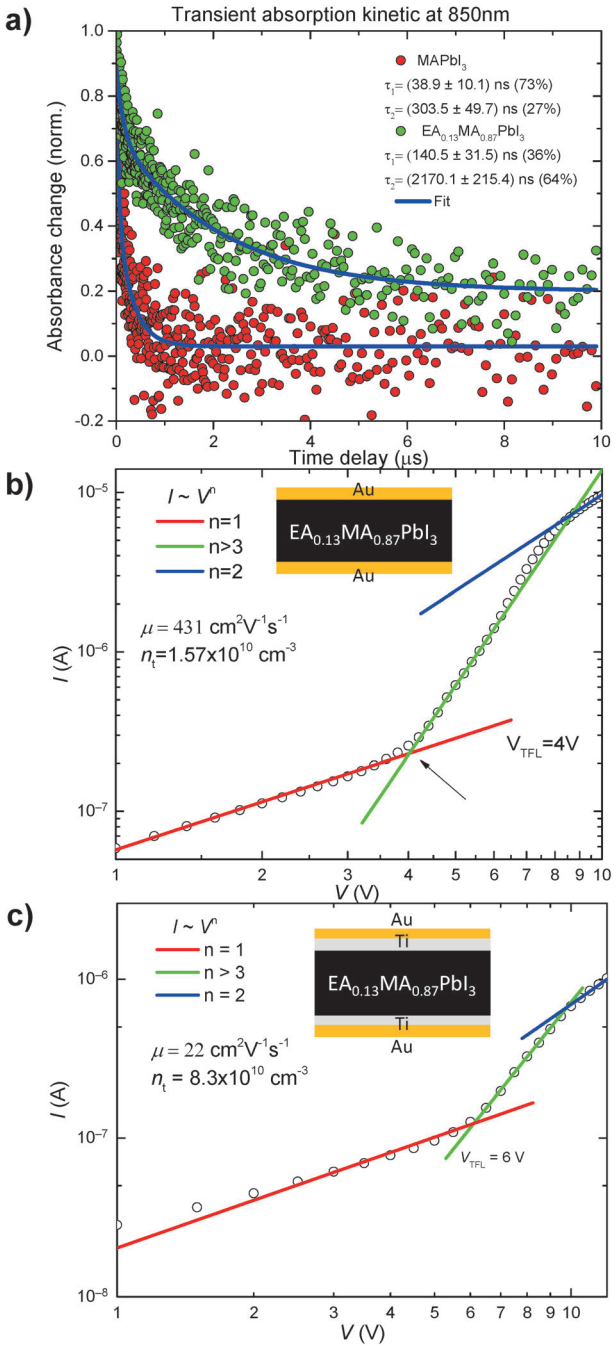

Figure 3. a) TA kinetics of $MAPbI_3$ and $EA_{0.17}MA_{0.83}PbI_3$ single crystals. The time constants of the fitting are listed. The *I–V* curve of b) Au/$EA_{0.17}MA_{0.83}PbI_3$ (dimension: 1.67×1.67×0.95 mm^3)/Au and c) Au/Ti/$EA_{0.17}MA_{0.83}PbI_3$ (dimension: 1.49×1.54×0.75 mm^3)/Ti/Au.

magnitude (see Figure S6 and also previous reports).[15,16] This result may also originate from the crystal symmetry improvement.[14b] The observation that the hole mobility is higher than the electron mobility can be partly ascribed to the fact that the defect density near the VBM is lower than that near the CBM, which is beneficial for reducing the scattering in charge transport. Complementarily, we measured the Hall effect mobility of the $EA_{0.17}MA_{0.83}PbI_3$ crystal and obtained a relatively smaller value of ca. 20 $cm^2V^{-1}s^{-1}$ for holes (Figure S7), possibly due to the surface probing characteristic of the Hall effect measurement and the condensed defects on the crystal surface.[9] It is worth mentioning that the lower bound of the diffusion length estimated with the worst cases of the mobility (20 $cm^2V^{-1}s^{-1}$) and the lifetime (300 ns) is 4 μm, still comparable with that of $MAPbI_3$ single crystals.[9] Therefore, although more detailed studies on the transport properties of $EA_{0.17}MA_{0.83}PbI_3$ are required, it holds great potential as an outstanding photovoltaic material.

So far, several routes to engineering hybrid perovskites have been reported, such as cation alloying and halide alloying.[1] However, most of the alloying choices have been limited to a few well-studied 3D perovskites. Our work opens a new direction in the crystal engineering of hybrid perovskites by revealing a strategy to incorporate relatively large cations, such as EA^+, in the perovskite 3D lattice through balancing lattice strains. This crystal engineering route was shown to modify various perovskite properties, such as crystal structure, stability, and optoelectronic properties. Our discovery suggests that the library of 3D alloy perovskites can be greatly expanded by introducing other large organic cations that may not form stable 3D perovskite structures by themselves.[2b] This approach provides intriguing possibilities to tune the structures and properties of the existing well-studied 3D perovskites.

Acknowledgements

This work was supported by King Abdullah University of Science and Technology (KAUST) in Saudi Arabia. W.P. thanks Dr. Yao He and Dr. Xiang Yu from Imaging and Characterization Core Lab (KAUST) for their assistance in the temperature-dependent XRD system set-up and measurement.

Keywords: crystal engineering · organic–inorganic hybrid composites · perovskite phases · photovoltaics

[1] a) T. M. Brenner, D. A. Egger, L. Kronik, G. Hodes, D. Cahen, *Nat. Rev. Mater.* **2016**, *1*, 15007; b) M. Grätzel, *Nat. Mater.* **2014**, *13*, 838 – 842 > ; c) W. Nie, H. Tsai, R. Asadpour, J.-C. Blancon, A. J. Neukirch, G. Gupta, J. J. Crochet, M. Chhowalla, S. Tretiak, M. A. Alam, H.-L. Wang, A. D. Mohite, *Science* **2015**, *347*, 822 – 825.

[2] a) D. B. Mitzi, *J. Chem. Soc. Dalton Trans.* **2001**, 1 – 12; b) G. Kieslich, S. Sun, A. K. Cheetham, *Chem. Sci.* **2015**, *6*, 3430 – 3433.

[3] a) D. H. Cao, C. C. Stoumpos, O. K. Farha, J. T. Hupp, M. G. Kanatzidis, *J. Am. Chem. Soc.* **2015**, *137*, 7843 – 7850; b) L. N. Quan, M. Yuan, R. Comin, O. Voznyy, E. M. Beauregard, S. Hoogland, A. Buin, A. R. Kirmani, K. Zhao, A. Amassian, D. H. Kim, E. H. Sargent, *J. Am. Chem. Soc.* **2016**, *138*, 2649 – 2655.

[4] T. A. Berhe, W.-n. Su, C.-H. Chen, C.-J. Pan, J. Cheng, H.-M. Chen, M.-C. Tsai, L.-Y. Chen, A. A. Dubale, B. J. Hwang, *Energy Environ. Sci.* **2016**, *9*, 323 – 356.

[5] B. Conings, J. Drijkoningen, N. Gauquelin, A. Babayigit, J. D'Haen, L. D'Olieslaeger, A. Ethirajan, J. Verbeeck, J. Manca, E. Mosconi, F. D. Angelis, H.-G. Boyen, *Adv. Energy Mater.* **2015**, *5*, 1500477.
[6] a) T. Baikie, Y. Fang, J. M. Kadro, M. Schreyer, F. Wei, S. G. Mhaisalkar, M. Graetzel, T. J. White, *J. Mater. Chem. A* **2013**, *1*, 5628; b) C. Quarti, E. Mosconi, J. M. Ball, V. D'Innocenzo, C. Tao, S. Pathak, H. J. Snaith, A. Petrozza, F. De Angelis, *Energy Environ. Sci.* **2016**, *9*, 155 – 163; c) M. T. Weller, O. J. Weber, P. F. Henry, A. M. Di Pumpo, T. C. Hansen, *Chem. Commun.* **2015**, *51*, 4180 – 4183.
[7] C. C. Stoumpos, C. D. Malliakas, M. G. Kanatzidis, *Inorg. Chem.* **2013**, *52*, 9019 – 9038.
[8] J.-H. Im, J. Chung, S.-J. Kim, N.-G. Park, *Nanoscale Res. Lett.* **2012**, *7*, 353.
[9] D. Shi, V. Adinolfi, R. Comin, M. Yuan, E. Alarousu, A. Buin, Y. Chen, S. Hoogland, A. Rothenberger, K. Katsiev, Y. Losovyj, X. Zhang, P. A. Dowben, O. F. Mohammed, E. H. Sargent, O. M. Bakr, *Science* **2015**, *347*, 519 – 522.
[10] T. Leijtens, G. E. Eperon, N. K. Noel, S. N. Habisreutinger, A. Petrozza, H. J. Snaith, *Adv. Energy Mater.* **2015**, *5*, 1500963.
[11] O. F. Mohammed, D. Xiao, V. S. Batista, E. T. J. Nibbering, *J. Phys. Chem. A* **2014**, *118*, 3090 – 3099.
[12] M. I. Saidaminov, A. L. Abdelhady, B. Murali, E. Alarousu, V. M. Burlakov, W. Peng, I. Dursun, L. Wang, Y. He, G. Maculan, A. Goriely, T. Wu, O. F. Mohammed, O. M. Bakr, *Nat. Commun.* **2015**, *6*, 7586.
[13] C. Motta, F. El-Mellouhi, S. Kais, N. Tabet, F. Alharbi, S. Sanvito, *Nat. Commun.* **2015**, *6*, 7026.
[14] a) F. Zheng, L. Z. Tan, S. Liu, A. M. Rappe, *Nano Lett.* **2015**, *15*, 7794 – 7800; b) A. Amat, E. Mosconi, E. Ronca, C. Quarti, P. Umari, M. K. Nazeeruddin, M. Grätzel, F. De Angelis, *Nano Lett.* **2014**, *14*, 3608 – 3616; c) J. Even, L. Pedesseau, J.-M. Jancu, C. Katan, *J. Phys. Chem. Lett.* **2013**, *4*, 2999 – 3005; d) T. Etienne, E. Mosconi, F. De Angelis, *J. Phys. Chem. Lett.* **2016**, *7*, 1638 – 1645.
[15] V. Adinolfi, M. Yuan, R. Comin, E. S. Thibau, D. Shi, M. I. Saidaminov, P. Kanjanaboos, D. Kopilovic, S. Hoogland, Z.-H. Lu, O. M. Bakr, E. H. Sargent, *Adv. Mater.* **2016**, *28*, 3406 – 3410.
[16] Q. Dong, Y. Fang, Y. Shao, P. Mulligan, J. Qiu, L. Cao, J. Huang, *Science* **2015**, *347*, 967 – 970.

Received: May 18, 2016
Published online: ■■ ■■, ■■■■

Communications

Hybrid Composites

W. Peng, X. Miao, V. Adinolfi, E. Alarousu, O. El Tall, A. H. Emwas, C. Zhao, G. Walters, J. Liu, O. Ouellette, J. Pan, B. Murali, E. H. Sargent, O. F. Mohammed, O. M. Bakr* _____ ■■■■–■■■■

Engineering of $CH_3NH_3PbI_3$ Perovskite Crystals by Alloying Large Organic Cations for Enhanced Thermal Stability and Transport Properties

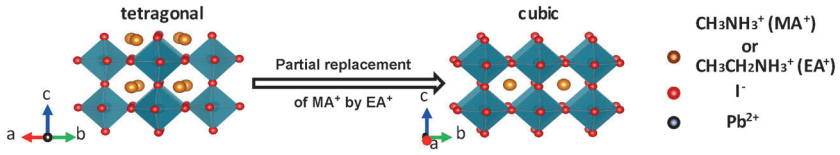

Despite its large ionic radius, ethylammonium can partially replace methylammonium in the widely studied 3D hybrid perovskites $CH_3NH_3PbI_3$. This partial replacement results in higher crystal symmetry, improved material stability, and markedly enhanced photocarrier lifetime of the alloy perovskites.